Original Article

JCBFM

Journal of Cerebral Blood Flow & Metabolism
2022, Vol. 42(5) 811–825
© The Author(s) 2021
Article reuse guidelines:
sagepub.com/journals-permissions
DOI: 10.1177/0271678X211062279
journals.sagepub.com/home/jcbfm
SAGE

High-resolution relaxometry-based calibrated fMRI in murine brain: Metabolic differences between awake and anesthetized states

Mengyang Xu[1,2,3,4,*], Binshi Bo[5,*], Mengchao Pei[5], Yuyan Chen[5], Christina Y Shu[6,7], Qikai Qin[1,2,4], Lydiane Hirschler[8,9], Jan M Warnking[8], Emmanuel L Barbier[8], Zhiliang Wei[10,11], Hanzhang Lu[10,11], Peter Herman[7,12,13], Fahmeed Hyder[6,7,12,13], Zhi-jie Liu[1,2,3], Zhifeng Liang[5] and Garth J Thompson[1]

Abstract

Functional magnetic resonance imaging (fMRI) techniques using the blood-oxygen level-dependent (BOLD) signal have shown great potential as clinical biomarkers of disease. Thus, using these techniques in preclinical rodent models is an urgent need. Calibrated fMRI is a promising technique that can provide high-resolution mapping of cerebral oxygen metabolism (CMR_{O2}). However, calibrated fMRI is difficult to use in rodent models for several reasons: rodents are anesthetized, stimulation-induced changes are small, and gas challenges induce noisy CMR_{O2} predictions. We used, in mice, a relaxometry-based calibrated fMRI method which uses cerebral blood flow (CBF) and the BOLD-sensitive magnetic relaxation component, R_2', the same parameter derived in the deoxyhemoglobin-dilution model of calibrated fMRI. This method does not use any gas challenges, which we tested on mice in both awake and anesthetized states. As anesthesia induces a whole-brain change, our protocol allowed us to overcome the former limitations of rodent studies using calibrated fMRI. We revealed 1.5-2 times higher CMR_{O2}, dependent upon brain region, in the awake state versus the anesthetized state. Our results agree with alternative measurements of whole-brain CMR_{O2} in the same mice and previous human anesthesia studies. The use of calibrated fMRI in rodents has much potential for preclinical fMRI.

Keywords

Awake mice, anesthesia, dexmedetomidine, calibrated fMRI, CMRO2, TRUST, pCASL

Received 26 April 2021; Revised 27 August 2021; Accepted 22 October 2021

[1]iHuman Institute, ShanghaiTech University, Shanghai, China
[2]School of Life Science and Technology, ShanghaiTech University, Shanghai, China
[3]Center for Excellence in Molecular Cell Science, Shanghai Institute of Biochemistry and Cell Biology, Chinese Academy of Sciences, Shanghai, China
[4]University of Chinese Academy of Sciences, Beijing, China
[5]CAS Center for Excellence in Brain Sciences and Intelligence Technology, Institute of Neuroscience, Chinese Academy of Sciences, Shanghai, China
[6]Biomedical Engineering, Yale University, New Haven, CT, USA
[7]Magnetic Resonance Research Center (MRRC), Yale University, New Haven, CT, USA
[8]Grenoble Institut des Neurosciences, Inserm, Univ. Grenoble Alpes, Grenoble, France
[9]C.J. Gorter Center for High Field MRI, Department of Radiology, Leiden University Medical Center, Leiden, The Netherlands
[10]Russell H. Morgan Department of Radiology and Radiological Science, Johns Hopkins University School of Medicine, Baltimore, MD, USA
[11]F. M. Kirby Research Center for Functional Brain Imaging, Kennedy Krieger Research Institute, Baltimore, MD, USA
[12]Quantitative Neuroscience with Magnetic Resonance (QNMR) Core Center, Yale University, New Haven, CT, USA
[13]Radiology and Biomedical Imaging, Yale University, New Haven, CT, USA

*These authors contributed equally to this article.

Corresponding authors:
Garth Thompson, iHuman Institute, ShanghaiTech University, 230 Haike Road, Pudong, Shanghai 201210, China.
Email: gthompson@shanghaitech.edu.cn

Zhifeng Liang, Institute of Neuroscience, CAS Center for Excellence in Brain Sciences and Intelligence Technology, Chinese Academy of Sciences, Shanghai, China.
Email: zliang@ion.ac.cn

Introduction

Functional magnetic resonance imaging (fMRI) is a key tool in understanding brain function. In particular, the commonly-used blood oxygenation level-dependent (BOLD) signal, can reveal both brain regions activated by tasks or stimuli, and communication among networks at rest.[1] Such networks, in particular, have been linked to a wide variety of neurological and psychiatric diseases, strongly suggesting the possibility of clinical translation for diagnosis or treatment planning.[2]

Complicating translation, however, is that the BOLD signal depends on the deoxyhemoglobin concentration ([dHb]) in a voxel which itself depends on complex interactions between cerebral blood flow (CBF), cerebral blood volume (CBV), and cerebral metabolic rate of oxygen (CMR_{O2}).[3,4] One way towards better understanding BOLD signal changes is to use rodent models so that genetic alterations and invasive measurements can be used.[5] In particular, it is important that methods which increase the number of metabolic parameters that MRI can measure, such as methods to separate CBF, CBV, or CMR_{O2} from the BOLD signal, can be translated to rodent models.

As neurons and glial cells require CMR_{O2} commensurate with their activity level[6–9] CMR_{O2} tracks functional brain activity and thus quantitative measurement of CMR_{O2} is a promising direction. Davis et al. and Hoge et al introduced a method designed to disassociate changes in CMR_{O2} from changes in CBF (or CBV) and BOLD signal, called "calibrated fMRI".[10,11] Currently, most calibrated fMRI methods involve "gas challenges" to induce changes in blood levels of O_2[12] and CO_2.[13] The gas challenge step induces either hyperoxia (inhalation of O_2) or hypercapnia (inhalation of CO_2). The latter is more commonly used since CO_2 is a potent vasodilator and thus can be used to estimate the maximum possible BOLD signal change, denoted as M.[10,11]

Because of the promise of calibrated fMRI, its implementation in preclinical rodent models is very important. However, several barriers exist:

1. In small animals the measurement of M by gas challenge is extremely noisy because of the small range of BOLD and CBF data points that are used to derive the equation parameters. To address this, prior work by Kida et al. and by Shu et al. indicated that estimation of M without a gas challenge was less noisy.[14,15] Several other methods can also estimate M without a gas challenge.[16–18]
2. Calibrated fMRI studies are often based on local sensory stimulation paradigms.[19] The changes observed in local sensory stimulation paradigms are small, both in terms of activation magnitude and spatial size. Thus they are more difficult to statistically locate on the small brains of rodents than in they are in humans (even at high magnetic fields). To address this, an alternative is to use an anesthesia paradigm to alter global brain activity.[20] This is similar logic to previous validation of CMR_{O2} changes from calibrated fMRI vs. CMR_{O2} changes from Carbon-13 Magnetic Resonance Spectroscopy.[14] The anesthetic dexmedetomidine has been used previously as a global paradigm in human CMR_{O2}[21] and CBF[22] studies, and can also be used in mouse fMRI.[23]
3. The vast majority of human fMRI studies (including calibrated fMRI) have used awake subjects, whereas the vast majority of animal fMRI studies have used anesthesia.[5] To bridge this gap, our previous work has developed an awake mouse fMRI model[24] and this was utilized in the current study.
4. These problems may compound. For example, Sicard et al. suggested that the neural response to a stimulus can be reduced by an anesthesia, and also the ability to measure it simultaneously reduced by loss of vascular reactivity due to a gas challenge.[25]

We used an extension of the calibrated fMRI method developed by Shu et al.[15] Shu et al. began this work in anesthetized rats[15] but (to our knowledge) this method has not been published on mice thus far. The derived M parameter (or specifically, the relaxation rate described below) from this method is no different than the M parameter derived from Hoge et al.'s deoxyhemoglobin-dilution model of CMR_{O2}.[11] It is based on the fact that the BOLD signal is captured differentially by two different transverse magnetic relaxation rates, R_2* which includes magnetic susceptibility components that can be reversed, and components that cannot be reversed, and R_2 which includes only magnetic susceptibility components that cannot be reversed. The M parameter can be modelled as the product of the fMRI echo time (TE) and R_2' (the BOLD-based magnetic susceptibility component that can be reversed, given by the difference between R_2* and R_2 under well-shimmed conditions).[18] We combine the R_2' measurement with a measurement of CBF to calculate a relative CMR_{O2} map ($rCMR_{O2}$) between states, which we refer to as relaxometry-based calibrated fMRI (rcfMRI). We applied this rcfMRI to the same mice in the awake[24] and dexmedetomidine anesthetized[23] states. We also assessed the power-law dependence between BOLD signal and [dHb], modelled as the exponent β.[26] Together, quantitative mapping of CBF and the M and β parameters allowed estimation of brain-wide $rCMR_{O2}$ changes induced by anesthesia from the awake state.

The map of $rCMR_{O2}$ between states displayed globally higher CMR_{O2} in awake versus anesthetized mice. Interestingly, we were also able to observe some regional differences in the global increase, including a cortical versus subcortical difference previously observed (using other techniques) in humans under dexmedetomidine.[22] Our $rCMR_{O2}$ result from rcfMRI was corroborated by a global CMR_{O2} change measured using an established method, T_2 relaxation under spin-tagging (TRUST) MRI,[27,28] an idea similar to the cortex-wide validation previously performed by Kida et al.[14]

The ability to apply rcfMRI in a preclinical model is critical for the translation of calibrated fMRI as a technique, so that it can be used for preclinical objectives such as assessing drug effects or testing mouse disease models. We have mapped $rCMR_{O2}$ on a voxel-by-voxel basis in awake mice, opening new avenues for preclinical studies.

Materials and methods

Summary of the overall method for rcfMRI

The overall method for rcfMRI is shown in Figure 1. Data were recorded in two states using the same sequences.

Theory

In this section, we describe the derivation of the equation we use to calculate $rCMR_{O2}$. This is an expansion of previous work by Kida et al.[14] which showed the basis of relaxometry-based calibrated fMRI method applied in rats.[15,29] We begin with the original model of the relationship between magnetic relaxation and deoxyhemoglobin concentration, shown in equation (E1),[11,30]

$$R_2' = A \cdot CBV \cdot [dHb]^{\beta} \tag{E1}$$

where R_2' is the (positive) increase in magnetic relaxation rate due to deoxyhemoglobin,[4,15,31] A is a field-dependent magnetic susceptibility constant,[30] CBV is the blood volume, and β is the exponent in the power-law dependence between BOLD signal and the deoxyhemoglobin concentration in blood ([dHb]) which depends on blood vessel size.[10] β and R_2' vary across different brain regions.[26] Ignoring all non-susceptibility terms that contribute to transverse relaxation, blood oxygenation (Y) induced intravoxel spin dephasing is reflected differently by gradient-echo (R_2^*) and spin-echo (R_2) relaxation rates

$$R_2^* = R_2'(Y) + R_2(Y) \tag{E2a}$$

$$R_2 = R_2(Y) \tag{E2b}$$

because R_2^* contains both reversible (e.g., static magnetic fields inhomogeneity, slow diffusion regime) and irreversible (i.e., intermediate to fast diffusion regime) terms and R_2 contains just the irreversible term.[14] Under well-shimmed conditions, we assume that the difference between R_2 and R_2^*, R_2', is greater than zero primarily due to deoxyhemoglobin, the BOLD-sensitive component.

$$R_2' = R_2^* - R_2 \tag{E2c}$$

For the purposes of our model, we only consider the deoxyhemoglobin-sensitive part of changes in R_2'. However, under poorly-shimmed conditions this may not hold as R_2' could be dominated by effects of the static magnetic field, B_0. The right side of E3a is taken from E1 with CBV being replaced by CBF to an exponential power. This is done using Grubb's constant α.[32] Note that this assumes that CBF follows CBV changes and vice-versa with a consistent functional relationship, not that either is necessarily passive. Finally, steady state deoxyhemoglobin concentration in the venous compartment is replaced with CBF and CMR_{O2}.[11]

$$R_2' = A \cdot [CBF]^{\alpha} \cdot \left[\frac{1}{4}\frac{CMR_{O2}}{CBF}\right]^{\beta} \tag{E3a}$$

$$CMR_{O2} = 4 \cdot \left(\frac{R_2'}{A}\right)^{\frac{1}{\beta}} \cdot \left(CBF\right)^{1-\frac{\alpha}{\beta}} \tag{E3b}$$

Previous work has shown that β is invariant across brain states[26] and the constant α is defined as a shift between two brain states.[11] Thus, defining CMR_{O2}, R_2', and CBF in two different states, represented by subscripts P and Q, we can derive equation (E4),

$$rCMRO_2 = \frac{CMRO_{2,P}}{CMRO_{2,Q}} = \left(\frac{R2'_P}{R2'_Q}\right)^{\frac{1}{\beta}} \cdot \left(\frac{CBF_P}{CBF_Q}\right)^{1-\frac{\alpha}{\beta}} \tag{E4}$$

where A, the only unmeasured field-dependent constant, cancels out. Thus we can model $rCMR_{O2}$ based on only R_2' and CBF in two brain states, with only the constants α and β remaining, both of which are potentially measurable. For further information on α and β, see "Constants of the metabolic model" in supplemental information.

Animals

All animal procedures were approved by the Animal Care and Use Committee of the Institute of

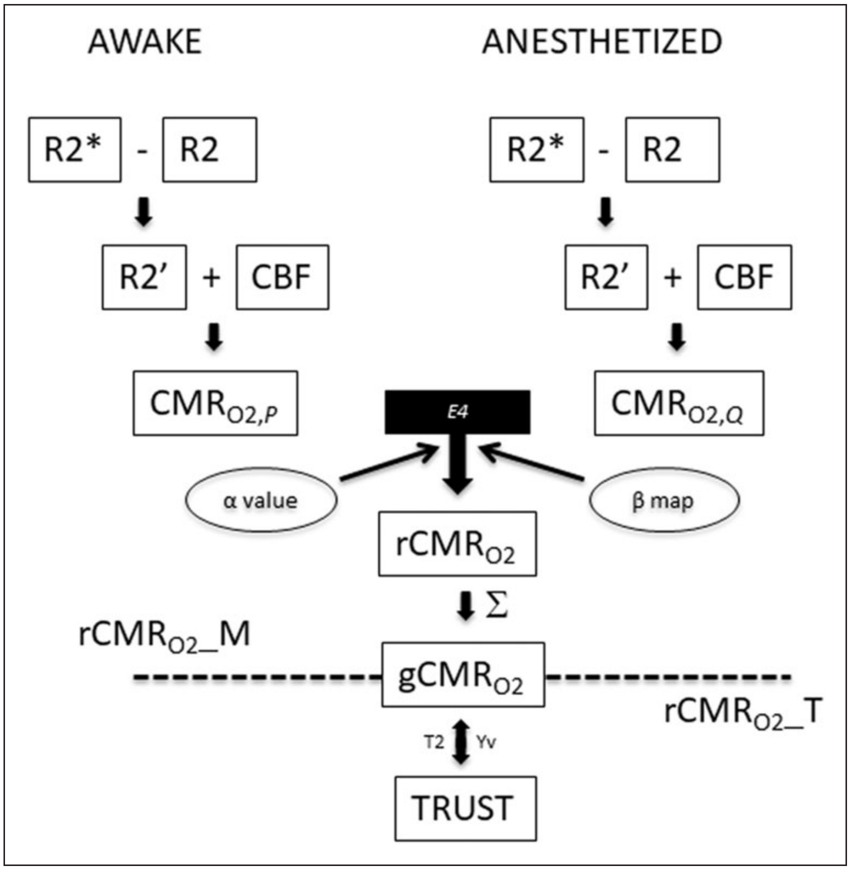

Figure 1. Summary of the overall method for rcfMRI. Data were recorded in the awake and anesthetized states using the same MRI sequences. The relaxation time map R_2' was calculated based on R_2 and R_2*, and combined with CBF in both states to calculate rCMR$_{O2}$ in the awake divided by the anesthetized state. rCMR$_{O2}$ was calculated using a range of values for the α constant, and a per-voxel map of the β constant which was measured experimentally. Global CMR$_{O2}$ (gCMR$_{O2}$) was calculated from this method (rCMR$_{O2}$_M), and also from TRUST MRI sequences by converting the T_2 measured with TRUST to venous oxygen saturation Y_v (rCMR$_{O2}$_T).

Neuroscience, Chinese Academy of Sciences, Shanghai, China (A), following "Laboratory animal – Guideline for ethical review of animal welfare" published by the People's Republic of China.[33,34] Animal data reporting herein follows the ARRIVE 2.0 guidelines.[35]

15 male adult C57BL/6 mice (Shanghai Laboratory Animal Center, Shanghai, China) of 7–9 weeks of age with weight 20–30 g were imaged in both awake and anesthetized states. Mice underwent awake imaging preparations identical to our previous studies.[24,36] Briefly, a head holder was attached to each animal's skull for head fixation, and animals were allowed to recover for one week after the surgery. Afterwards, animals were habituated for awake imaging over one week. The same mice were first imaged in the awake condition, and then again approximately one week later in the anesthetized condition. This order was maintained as we were concerned that dexmedetomidine exposure and recovery in the same setup as awake imaging would induce trauma if awake imaging was done later. Mice were labeled by cropped ear to match the same mouse between conditions. Initial examination of 4 mice indicated a strong effect in every mouse tested, but n = 15 was chosen to avoid under-sampling. 22 mice were tested in total. 5 mice died prior to completion of the experiment and were excluded, and 2 mice had physiological parameters outside of the acceptable range, so were also excluded; these criteria were established a priori. Mice were euthanized following the second (dexmedetomidine) scanning session.

Image acquisition

For both awake and anesthetized imaging sessions, mice were given 20% O_2/80% air mixture ("medical air" with total ~37% O_2 concentration), and respiration was monitored through a pneumatic pillow (SAII, Stony Brook, NY, USA). For anesthetized imaging sessions, mice were initially anesthetized using isoflurane (3.5% for induction, 1.5% during set-up) and a bolus of 0.025 mg/kg dexmedetomidine was given by intraperitonial injection. Isoflurane was discontinued after 5 min. Continuous subcutaneous infusion of dexmedetomidine at a dose of 0.05 mg/kg/h was started 10 min after the bolus injection. While under anesthesia, body temperature was monitored through a rectal probe and maintained at $37.0 \pm 0.5\,^{\circ}C$ using a warm water pad. Respiratory rate was between 262–293 breaths per minute while awake and between 142–158 breaths per minute while anesthetized.

MRI data were acquired with a Bruker BioSpec 9.4 T scanner, using an 86-mm volume coil (Bruker) for transmit and a 4-channel phased-array cryogenic mouse head coil (Bruker) for receive. After a Localizer scan for animal positioning, T_2 RARE anatomical images were acquired (TE 33 ms, TR 3300 ms, FOV 16×16 mm, matrix size 256×256, slice thickness 0.5 mm, number of slices 20, averages 2). The scanner adjustment took >3 min and the localizer and T2 RARE took >7 min. When combined with setup time, and time taken for physiology to stabilize, at least 30 minutes passed between the bolus injection and when calibrated fMRI scans began. As previous studies measuring CMR_{O2} with ^{15}O positron-emission tomography (PET) techniques have assumed CBF is relatively stable for at least 15 min to complete scanning,[37,38] and approximately 15–30 minutes is sufficient for a steady state of the vasculature after administering dexmedetomidine,[39] we assume a relatively steady state under our experimental protocol.

The relaxometry-based calibrated fMRI (rcfMRI) experiment consisted of measurement of CBF, a T_2 map, and a T_2* map. A pseudo-continuous arterial spin labeling (pCASL) sequence,[40] including label and control prescans to adjust the phase, was used to measure CBF (TE 22 ms, TR 4000 ms, matrix size 71×71, in-plane resolution 0.225×0.225 mm, slice thickness 0.5 mm, 20 slices, label duration 3 s, post labeling delay 300 ms, 80 pairs of label/control volumes). All pCASL sequences used 0.59 inversion efficiency, which was measured on the MRI prior to beginning this experiment as per Hirschler et al.[40] After field-map-based local shimming within the mouse brain (Figure S1), T_2* and T_2 maps were acquired with MGE (Multiple Gradient Echo, TR 500 ms, TE 2.15-17.23 ms, echoes 8, averages 4, slice thickness 0.5 mm, number of slices 20, FOV 22×16 mm, matrix size 110×80) and MSME (Multi Slice Multi Echo, TR 3000 ms, TE 10-100ms, echoes 10, averages 1, slice thickness 0.5 mm, number of slices 20, FOV 22×16 mm, matrix size 110×80) sequences. Finally, a mouse-optimized T_2-relaxation-under-spin-tagging (TRUST) sequence[28] was used to assess the T_2 of venous blood (TE 5.9 ms, TR 5000 ms, inversion slab thickness 1.5 mm, PLD 600 ms, FOV 16 mm $\times$ 16 mm, matrix size 128×128, slice thickness 0.5 mm, eTE values: 0.27, 7.5, 15 ms).

A separate, anesthetized, cohort of four mice without head holder implantation were used for quantifying β maps based on a previously reported method.[26] Mice were anesthetized using isoflurane followed by dexmedetomidine identical to the main cohort's anesthetized state (described above). Mice received three intravenous bolus injections of superparamagnetic contrast agent Molday (BioPAL Inc., Worcester, MA, USA, incremental dose of 5 mg/kg). Prior to injecting contrast agents and following each injection, T_2* and T_2 maps were acquired respectively with the same parameters as within the main cohort (described above). This separate cohort of mice was euthanized following scanning. Shu et al. discovered that β maps were consistent between two very different anesthetics which both have completely different mechanisms of action and also induce very different levels of sedation.[26] In addition, the β mapping experiment would have been very difficult to perform in awake mice due to its invasive nature. Thus, we assumed stable β maps between the awake and anesthetized conditions.

Data processing

Data were preprocessed using custom-written scripts in *MATLAB* and SPM12 (http://www.fil.ion.ucl.ac.uk/spm/). After the pCASL images were converted from Bruker format to NIFTI format, the mouse brain was extracted manually using ITK-SNAP (http://www.itksnap.org/), realigned for motion correction, normalized to a mouse brain template[74] (http://imaging.org.au/AMBMC/Model), and spatially smoothed (0.4 mm isotropic Gaussian Kernel) for quantifying CBF.[41]

The T_2* and T_2 maps were calculated using the normalized magnitude multi-echo MGE and MSME data with a mono-exponential fit by using the Levenberg-Marquardt algorithm. R_2' images were calculated using E2.[14]

To test data normality, we used Kolmogorov-Smirnov (KS) tests. The Lilliefors adjustment was used where $N \leq 15$. Most results are presented per-voxel (each voxel averaged across all mice) to follow previous studies of CMR_{O2} in humans.[42] In addition to per-voxel results, per-mouse results were also calculated. In per-mouse results, to test statistical significance in maps of CBF and R_2, the mean value of the map for each mouse was taken in 15 different brain regions (see Table S1). A two-tailed, paired *T*-test was done for each region, counting each mouse as a sample and pairing awake vs. anesthetized in that mouse. Resulting *p* values were corrected for multiple comparisons using Sequential Goodness of Fit[43] at $p \leq 0.05$, considering each brain map as a statistical family with 15 tests within it.

β maps were calculated using a previously published method[26] in *MATLAB*. By measuring R_2' as a function of the contrast agent concentration, β was experimentally determined on a voxel-by-voxel basis.

A per-voxel rcfMRI was calculated from E4 using maps of R_2' from each state, maps of CBF from each state, $\alpha = 0.2$, and the β map calculated from a separate cohort of mice. All results were normalized to the template described above. For further analysis, after registration, only slices 5-16 were selected due to image distortion induced by the head holder. A manual mask was applied to the final result by using the *roi_poly* function on each slice in *MATLAB* to exclude any artifacts along the edge of the brain. This helped maintain assumptions of our model by avoiding the higher inhomogeneity of the static magnetic field (B_0) at the edge of the brain. In addition, only the 5th through 16th slices were used for analysis, to avoid possible B_0 inhomogeneity at the far rostral and caudal extents of the brain.

For TRUST data, subtraction between the control and label images was performed.[28] A region of interest (ROI) was manually drawn on the difference image to encompass the sinus confluence at the superior sagittal sinus, then a mono-exponential fitting of the difference signal yielded a T_{2v} (venous T_2) estimation. A student's *t*-test was performed to compare T_{2v} under different conditions with a statistical threshold of $P < 0.05$.

"Global" $rCMR_{O2}$ was calculated for both rcfMRI results and TRUST results, referred to respectively as $rCMR_{O2}$_M and $rCMR_{O2}$_T. To calculate $rCMR_{O2}$_M, we used the relaxometry-based calibrated fMRI map (as described above, calculated on a per-voxel basis), and took the average from a conservative estimate of voxels known to be within the watershed area of the superior sagittal sinus based on existing atlases (Figure S2),[44,45] from the mouse brain template. (This area was chosen to match the TRUST results as closely as possible.) To calculate $rCMR_{O2}$_T, we used the T_2 values from TRUST, as described above, converted it to oxygen content of venous blood (Y_v) as per Lu et al,[27] then, to match methods described elsewhere,[19] we used the CBF data averaged from the watershed area (Figure S2) from the pCASL sequence described above to convert it to $rCMR_{O2}$, based on the Fick principle. (A full derivation is given in Supplemental Information.) The watershed areas were used instead of the whole brain as we hypothesized these areas had the greatest effect on TRUST results.

Mice with values for either $rCMR_{O2}$_T or $rCMR_{O2}$_M greater than 2 standard deviations from the respective group mean were removed. (Note: this was done only for the comparison analysis.) This resulted in removal of one mouse, leaving $N = 14$. The comparison analysis included both a test based on linear similarity, Pearson correlation, and a test which can also find non-linear similarities, mutual information (base 2 for logarithms, 5 bins of values), to compare $rCMR_{O2}$_T and $rCMR_{O2}$_M. Statistical significance for Pearson correlation was calculated using the permutation test from the built-in *corr* function in *MATLAB*. Statistical significance for mutual information was calculated by randomly permuting which mouse's $rCMR_{O2}$_T corresponded to which mouse's $rCMR_{O2}$_M and calculating mutual information between them for 100,000 random permutations. A one-tailed *p* value was calculated using the distribution of the randomized data to calculate a percentile, assuming the mutual information of the actual data was greater than the randomized data.

Results

Measurement of R_2' and CBF

Brain maps of the parameters measured in our experiment are displayed in Figure 2. We measured relaxation times R_2 ($1/T_2$) (Figure 2(b)) and R_2^* ($1/T_2^*$) (Figure 2(c)). R_2' (Figure 2(d)) was calculated as per E2. CBF was measured using pCASL (Figure 2(e)). R_2 and CBF maps showed a statistically significant difference in some brain regions (Table S2) with shorter R_2 (indicating longer T_2) and higher CBF in the awake condition versus the anesthetized condition. R_2^* and R_2' maps did not show a statistically significant difference between awake and anesthetized.

We compared our mouse CBF results to a previous study of CBF in awake versus dexmedetomidine-anesthetized human subjects which used PET.[22] Similar to humans, mice show a greater change from awake to anesthetized in the subcortex than the cortex, with the ratio being very similar between the two species (Table S3).

α and β constants

The α constant, representing the exponential power relationship between CBV and CBF, was primarily set to 0.2 to follow the original literature in human subjects,[46,47] measurements of the non-activated state in rats,[46,48] and finally because this later gave a good correspondence between rcfMRI and TRUST (see "Comparison of $rCMR_{O2}$ from rcfMRI and rCMRO2 from TRUST" below). However, as α has not been directly measured in mice, we also tested the full range of 0.1–0.4[29] in increments of 0.1 (see "Effect of varying of α on rcfMRI" below).

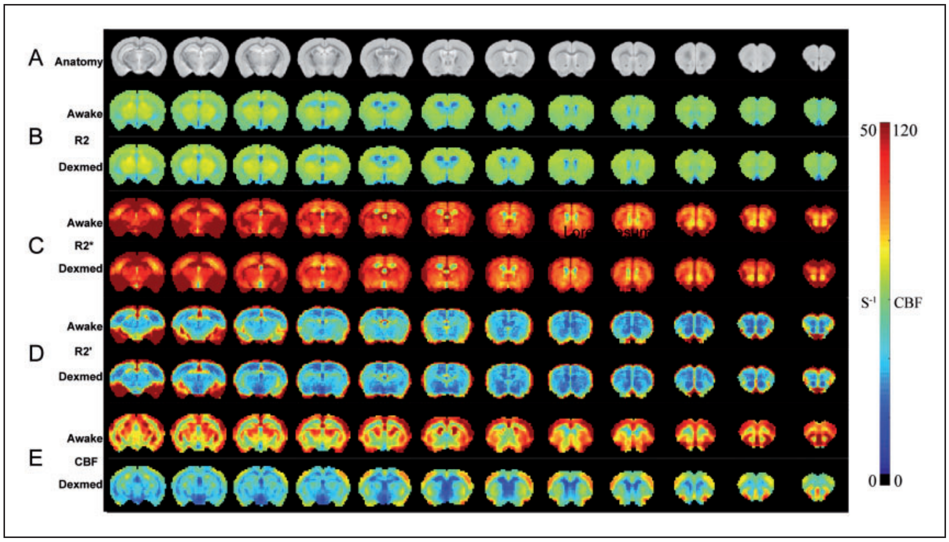

Figure 2. Comparison of R_2, R_2*, R_2' and CBF maps in awake and anesthetized states. Average brain maps of measured parameters. A. The 5th to 16th coronal slices from co-registered anatomical data. In B-E Mean values from awake and anesthetized groups ($N = 15$ mice) are shown on the top and bottom of each map respectively. B. R_2 relaxation time indicating transverse relaxation with refocused inhomogeneities. C. R_2* relaxation time with non-refocused inhomogeneities. D. R_2' relaxation time of only the inhomogeneities (see E2) E. Cerebral blood flow (CBF) generated using pCASL. Units are s^{-1} for relaxation maps, mL/100g/min for CBF.

The β constant, representing the non-linear susceptibility change due to deoxyhemoglobin, was measured using a previously published method,[26] which requires multiple injections of the contrast agent Molday. Figure 3(a), first four rows, shows the R_2' maps up to the third dose of Molday (mean of $N = 4$ mice). After each dose, R_2' increased substantially. β maps were generated based on the dose-relaxation curve, and are shown in the last row of Figure 3(a). Eight anatomical regions were chosen as ROIs, to represent the major areas based on a mouse brain atlas (http://atlas.brain-map.org/). See Table S1 for a list of ROIs and Figure S3 for locations of different ROI. ROI-specific quantification is shown in Figure 3(b).

For further information regarding α and β, see "Constants of the metabolic model" in supplemental information.

Measurement of $rCMR_{O2}$ using rcfMRI

Using the rcfMRI method, we used measurements of R_2' and CBF with constants α and β, and calculated $rCMR_{O2}$ based on E4. Figure 4(a) shows the mean $rCMR_{O2}$ map ($N = 15$ mice) in the awake divided by the anesthetized state. 96.7% $rCMR_{O2}$ voxels are >1, indicating that CMR_{O2} is globally higher in the awake state versus the anesthetized state. Furthermore, we observed this increase as appearing to be non-uniform across the brain. ROI-based analysis (Figure 4(b), see Figure S4 for ROI locations in gray-scale) suggests a higher ratio in subcortical regions than cortical regions, and more variation in $rCMR_{O2}$ among cortical regions. The trend of higher subcortical than cortical $rCMR_{O2}$ was present in 13 out of 15 mice. Voxel values within each brain region were significantly non-normally distributed ($p \leq 0.034$, KS test with Lilliefors adjustment). A Wilcoxon's rank sum test indicated that Cortical $rCMR_{O2}$ values were found significantly lower than the subcortical regions ($p = 0.0062$, mean of cortical regions $= 1.64$, mean of subcortical regions $= 2.11$). The auditory cortex exhibited the greatest change among the cortical ROIs, potentially indicating a higher baseline neural activity level in the awake state due to the conscious processing of acoustic noise during imaging. Indeed, a Wilcoxon's rank sum test indicated that the $rCMR_{O2}$ value of the auditory cortex was significantly higher than other cortical regions ($p = 0.0344$, mean of AUD $= 2.26$, mean of other cortical regions $= 1.61$).

Effect of varying of α on rcfMRI

To the best of our knowledge, α has not been directly measured in mice (and such a measurement is substantial work, beyond the scope of our study). Thus, we tested four different values for alpha from 0.1 to 0.4 based on the possible range[29] for calculating $rCMR_{O2}$ using the rcfMRI method (as was done above in "Measurement of rCMRO2 using rcfMRI" for $\alpha = 0.2$). These results are shown in Figure S5. While greater values for α produced slightly lower $rCMR_{O2}$ values, results were generally similar across the full range of α. No value of α changed our result of

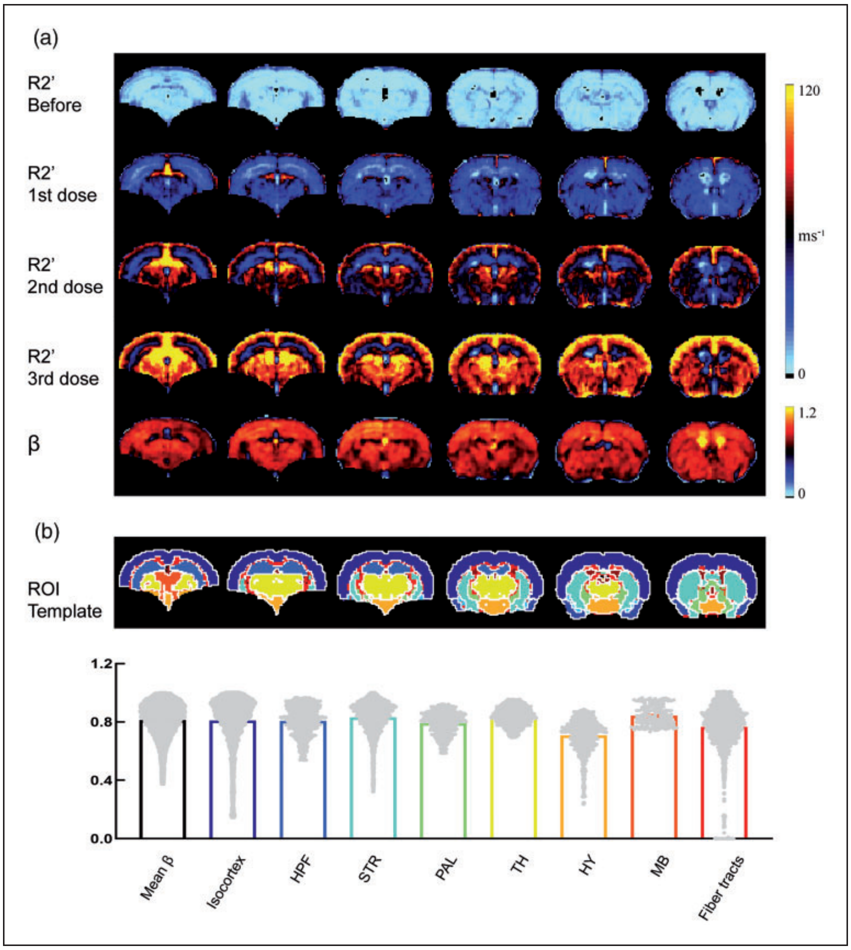

Figure 3. Dose-dependent R_2' for β-mapping. A. Mean R_2' images from four mice ($N = 4$) before, and after one, two, and three doses of Molday, to which β was fitted. B. Top row, ROI definition, bottom row, [5%,95%] mean β values distribution from each ROI. The colored outline of the bar matches the color of the equivalent ROI. One dot shown per voxel. The mean value for all shown regions is 0.80. Full ROI names are given in Table S1. Compare to Shu et al., 2016 Figure 3.[26] (See Figure S3 for ROI locations in grayscale).

observing a non-uniform, whole-brain increase in the awake condition versus the anesthetized condition.

Measurement of T_{2v} using TRUST

To validate the rcfMRI method, we used a different MRI method, TRUST,[27] to measure global oxygen metabolism in the awake and anesthetized states, in the same mice and imaging sessions where we measured rcfMRI. TRUST works by the subtraction of a control from a labeled image at multiple TE values, as shown in Figure 5(a), left side. Then, a monoexponential fitting of the signal intensity as a function TE yields the T_2 relaxation time of pure venous blood (T_{2v}), as shown in Figure 5(a), right side.

We observed a change in the mean T_{2v} in the awake condition ($T_{2v} = 6.84 \pm 1.53$ ms, mean ± SD.) when compared to the anesthetized condition ($T_{2v} = 5.80 \pm 1.34$ ms, mean ± SD.). T_{2v} in each condition was potentially normally distributed ($p > 0.05$, KS test with Lilliefors adjustment). This change was statistically significant (paired *T*-test, one tail assuming the same direction as rcfMRI: awake > anesthetized, $p = 0.025$, $T = 2.14$).

Comparison of $rCMR_{O2}$ from rcfMRI ($rCMR_{O2}$_M) and $rCMR_{O2}$ from TRUST ($rCMR_{O2}$_T)

To directly compare between rcfMRI and TRUST, both were converted into global $rCMR_{O2}$ measurements. For the former, the mean value for all voxels in the watershed area of the superior sagittal sinus (Figure S2)[44,45] was taken from the mean ($N = 15$ mice) $rCMR_{O2}$ map created using the rcfMRI method. This was referred to as $rCMR_{O2}$_M. For the latter, values for T_{2v} were first converted to Y_v as per Lu et al.,[27] shown in Figure 5(b). Y_v was $61.0 \pm 4.8\%$ for awake and $57.6 \pm 5.4\%$ for anesthetized (mean ± SD., same test as T_{2v} above, $p = 0.039$, $T = 1.90$). Mean CBF values from the watershed area (Figure S2) for each mouse and each state are shown in Figure 5(c).

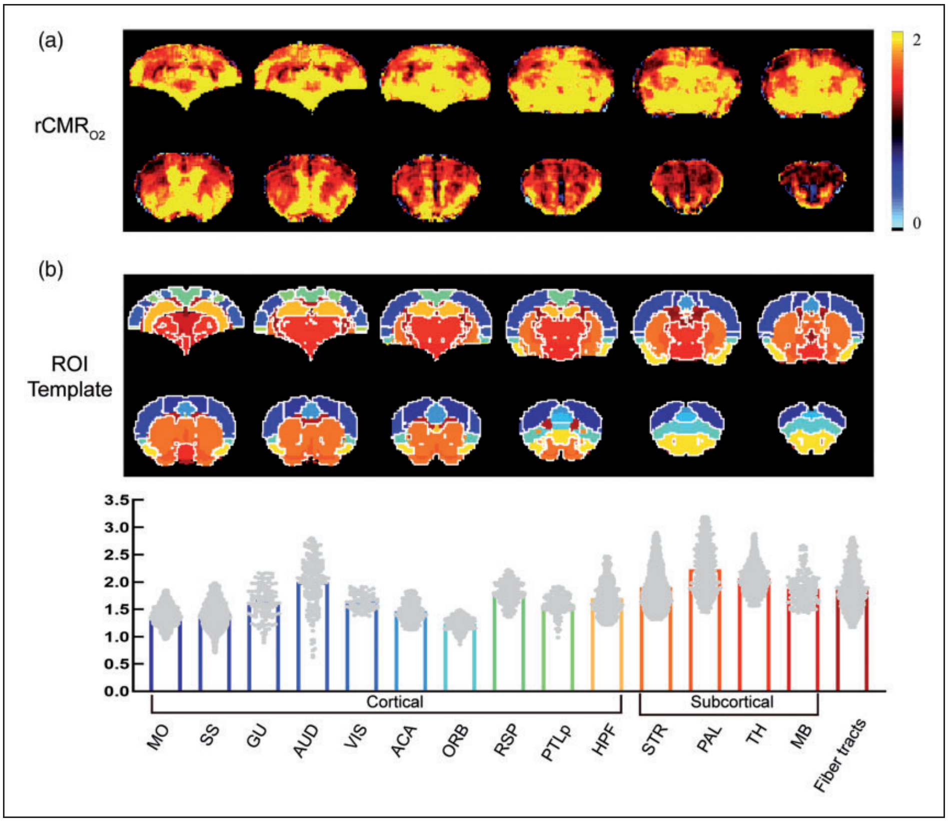

Figure 4. Relative CMRO$_2$ (rCMRO$_2$) image results and regional analysis. A. rCMR$_{O2}$ map calculated using the rcfMRI method, for the awake condition divided by the anesthetized condition (mean of N = 15 mice). Note that there is a global increase in the awake condition. B. Top row, ROI definitions, bottom row, [5%,95%] ROI-wise mean values distribution for rCMRO$_2$. The colored outline of the bar matches the color of the equivalent ROI. One dot shown per voxel. While there is a global increase, it does not appear to be uniform across the brain, or even appear to be uniform across the cortex. Full ROI names are given in Table S1. (See Figure S4 for ROI locations in grayscale).

CBF was 90.1 ± 7.3 mL/100g/min for awake and 52.3 ± 10.1 mL/100g/min for anesthetized (mean $\pm$ SD., same test as T_{2v} above, $p = 5.66 \times 10^{-9}$, $T = 11.8$). Combining Y_v and whole-brain CBF, as per Ciris et al. and Lu et al.,[27,49] we obtained global rCMR$_{O2}$ from TRUST. This was referred to as rCMR$_{O2}$_T (Figure 5(d)).

The mean value for the rCMR$_{O2}$_T is 1.63 ± 0.33 while rCMR$_{O2}$_M's mean value is 1.52 ± 0.36 (Mean $\pm$ SD.) at $\alpha = 0.2$. rCMR$_{O2}$_M and rCMR$_{O2}$_T were significantly non-normally distributed ($p \leq 0.032$, KS test with Lilliefors adjustment). Due to this non-normality, we decided to compare both linear similarity (Pearson correlation) and similarity which includes non-linearity (Mutual Information).

Comparison analysis was not statistically significant for linear similarity measured with Pearson correlation, but was statistically significant when non-linear similarities were considered using mutual information. Pearson correlation between rCMR$_{O2}$_T and rCMR$_{O2}$_M on a per-mouse basis was $r = 0.23$, this was not statistically significant ($p = 0.43$). Mutual information was 1.5 for actual data, with a median of 1.1 for random data with 5th percentile of 0.80 and 95th percentile of 1.4, resulting in $p = 0.013$. This suggests a statistically significant, but non-linear relationship between CMR$_{O2}$ as measured with TRUST and CMR$_{O2}$ as measured with calibrated fMRI.

Discussion

Main findings

Calculating rCMR$_{O2}$ maps using relaxometry-based calibrated fMRI (rcfMRI) required measurement of relaxation time R_2' and CBF for the same mouse subject, as well as the parameters α, which we tested across a range, and β, which we measured in a separate cohort of mice. We succeeded in measuring R_2' and CBF in 15 mice in both the awake and anesthetized states.

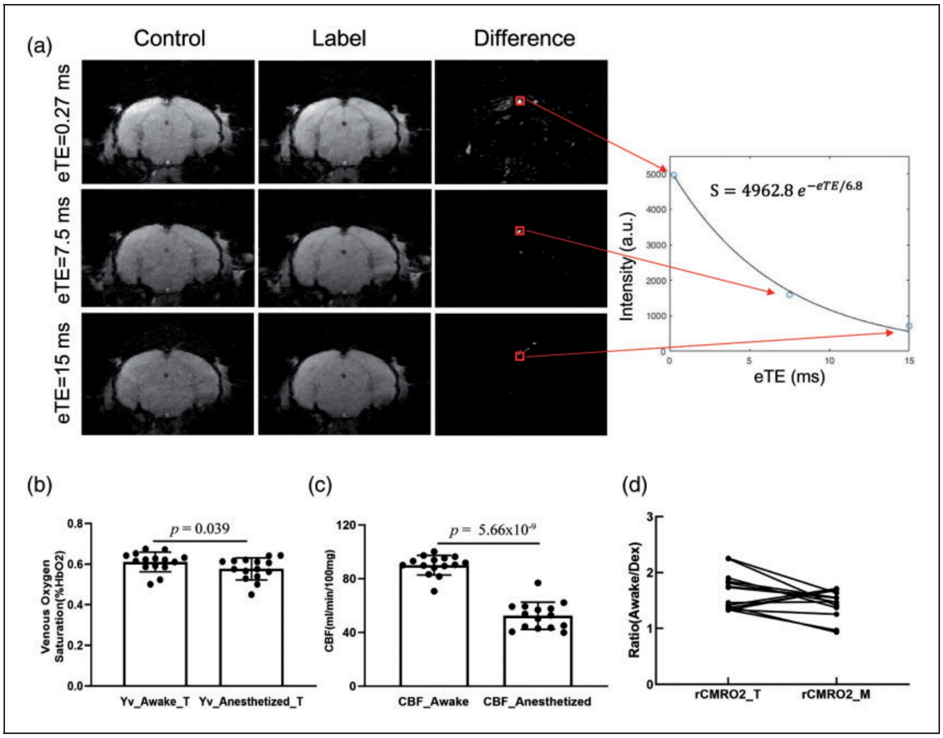

Figure 5. TRUST global $rCMR_{O2}$ agrees with rcfMRI. A. Illustration of the TRUST method using a representative mouse from our study. The signal was calculated within the sinus confluence of the superior sagittal sinus at different echo times to allow the calculation of T_{2v} from regions which drain from it. B. Comparison of Y_v converted from T_{2v} between awake and anesthetized states (N=15), mean±SD for venous oxygen saturation. One dot shown per mouse. C. Comparison of CBF values between awake and anesthetized states(N=15), mean±SD with error bar. One dot shown per mouse. D. Comparison between global $rCMR_{O2}$ from TRUST ($rCMR_{O2}$_T) and averaged rcfMRI result from the superior sagittal sinus ($rCMR_{O2}$_M). (N = 14) (Scatter plot shown in Figure S6).

Considering awake versus anesthetized states, we observed globally higher $rCMR_{O2}$ in the awake state. Moreover, the increase we observed was non-homogenous; the cortex showed a trend of a smaller change than the subcortex with high $rCMR_{O2}$ in auditory cortex. The observation of globally higher $rCMR_{O2}$ in the awake state versus an anesthetized state follows many previous studies which used PET to measure glucose metabolism or CBF in human subjects given anesthetics.[7,50–55] While care must be taken as gray matter/white matter balance differences between the cortex and the subcortex may alter signal-to-noise (SNR) of our measurements, the difference in the change between cortical and subcortical regions matched previous studies of dexmedetomidine anesthesia in humans (Table S3).[22,56]

Interestingly, while our work indicates that rcfMRI can measure the metabolic shift from awake to anesthetized, we also found a non-linear relationship between rcfMRI and TRUST $rCMR_{O2}$ results. Results from TRUST were in the same direction as from rcfMRI (Figure 5(d)), but the two global measurements only had a weak linear relationship on a per-mouse basis. There was, however, a statistically significant non-linear relationship between global $rCMR_{O2}$ measurement with TRUST versus with rcfMRI. This suggests that modeling deoxyhemoglobin from susceptibility changes may be more complex than expected for $rCMR_{O2}$_M by rcfMRI. Whereas some speculation is given in Figure S6 for $rCMR_{O2}$_T by TRUST due to variable inflow to large vessels, to understand this non-linear relationship will require further study.

Effects of anesthesia, and CBF

We chose anesthesia as a method of creating a large alteration to brain metabolism.[14] Anesthesia affects neural activity in an agent- and dose-dependent manner. Most anesthetic agents, including dexmedetomidine, suppress neural activity (though other anesthetic agents, such as midazolam, did not significantly).[20,56,57] Studies done in rodents using ketamine-xylazine and urethane-xylazine have shown disturbances to temperature, heart rate, and breath rate, stressing the importance of maintaining physiological parameters under anesthesia.[58] Studies done in rodents under isoflurane, (where dose may be easily altered) have shown a strong dose-dependence on the neural suppression induced by anesthesia.[59]

Our calibrated fMRI method attempts to model CMR_{O2}, and thus does not distinguish CMR_{O2} changes due to purely vascular vs. purely neural activity, both of which can be induced by anesthesia. Vascular effects of dexmedetomidine are relatively stable 30 minutes after the bolus injection.[39] Thus we expect vascular changes we observed to be due to the relatively stable state which the anesthesia elicits.

A recent meta-analysis investigated human PET studies which measured glucose metabolism[60] suggested that results from studies which used anesthesia were dominated by a global decrease in glucose metabolism in the anesthetized state. As cerebral glucose and cerebral oxygen metabolism are tightly coupled,[42,61] our results support this observation. Indeed, Qiu et al., who measured neural activity directly, did observe a decrease under dexmedetomidine.[57,62,63] While this may suggest an effect which is not agent-specific,[60] possibly due to reduced neural activity, dexmedetomidine hypothetically may also bind to α2-adrenergic receptors in vasculature.[64] If this is occurring, some of the vasoconstriction under dexmedetomidine could be caused by this effect, in addition to vasoconstriction caused by reduced neural activity.

Also consider relative CBF (rCBF), calculated by dividing CBF in the awake state by the anesthetized state, shown in Figure S7. rCBF shows a global trend similar to $rCMR_{O2}$, as would be expected from human dexmedetomidine studies,[21] however rCBF has less variation between brain regions as it lacks the influence of the deoxyhemoglobin-sensitive component R_2'.

Anesthesia is used in most animal fMRI studies.[65] However, local metabolic differences between awake and anesthetized states are rarely considered. By using dexmedetomidine, which is an agonist of α2-adrenergic receptor,[66] we were able to examine this difference in the mouse brain. In addition to globally lower CMR_{O2} in the anesthetized state, regional variability was also apparent. While we speculate some variability may be due to conscious processing of stimulus while awake (e.g. activation of auditory cortex shows a significant difference, likely due to scanner noise), overall the sources of regional variability may be highly complicated. We speculate that one of these sources may be variation of α2-adrenergic receptor expression levels across the brain, as has been observed using genetically-encoded calcium imaging,[62] and seen in human studies of CBF.[22] This may cause differential reductions in information processing, or differential vascular effects, due to the dexmedetomidine. Future studies comparing multiple anesthetics with the awake state would be needed to clarify this, though independent measurement of CBV may be needed for anesthetics which alter vasculature tone, such as isoflurane.[67] Finally, while mice did undergo habituation prior to the experiment, the awake state may still be stressful, which could affect oxygen metabolism versus true "awake resting" as well.

rcfMRI in context of other MRI-based CMR_{O2} measurements

As measuring the change in cerebral oxygen metabolism is a quantitative way to measure neural activity at a whole-brain scale, many MRI-based methods of quantifying CMR_{O2} have been developed. These can be classified as extravascular methods, which include most calibrated fMRI methods, and intravascular methods, such as the TRUST method used in our study.[19] Calibrated fMRI methods can also be divided into gas-challenge and gas-free calibrated fMRI. Traditional calibrated fMRI required a gas challenge to determine M. This was done either by applying hypercapnia through administering CO_2 to subjects, or (less commonly) applying hyperoxia through administering O_2 to subjects.[19] High levels of CO_2 or low levels of O_2 can suppress the ability to measure neural activity as vascular reactivity is lost. This may thus present a particularly difficult problem in animals under anesthesia, as the anesthesia has already lowered the level of neural activity.[25] In addition, even at CO_2 levels and stimulation levels where gas challenges are effective, they may create problems for translation including the potential for anxiety or panic,[68] and altered electroencephalogram rhythms,[69,70] which creates a risk for patients with neurological conditions. Altered neural activity is also a problem from a scientific perspective; in addition local activity is also altered.[71,72]

Recently-developed gas-free calibrated fMRI methods, including the rcfMRI method we used, are exciting as they may provide a way to apply calibrated fMRI broadly. Our work used the method developed by Shu et al.[15] A similar method to Shu et al. was used by Göttler and Kaczmarz et al. who calculated $rCMR_{O2}$ based on using R_2' and independent CBV and CBF measurements to find the oxygen extraction fraction (OEF).[73] Berman et al. used a gas-free calibrated fMRI method which has similar assumptions to Shu et al. (see E3a in the present study), but instead of measurement of traditional R_2 and R_2* maps they quantified R_2' at multiple echo times using asymmetric spin echo sequences.[16] It is worth noting that the asymmetric spin-echo sequences used in Berman et al. to record R_2 maps underestimated the R_2' value, whereas standard spin-echo EPI sequences (including the MSME sequence we used) do not appear to underestimate R_2'. However, standard spin-echo EPI sequences have more heterogeneity than non-EPI sequences as per Figure 4 from Shu et al.[15] Thus the choice of the relaxometry sequences will influence measurement of R_2' and be a tradeoff versus time, accuracy, and under- or over- estimation.

Conclusion

We were able to successfully use rcfMRI in awake and anesthetized mice to observe the global metabolic shift due to dexmedetomidine anesthesia. As expected based on human studies, the anesthetized state was lower than the awake state. This global shift was recapitulated with TRUST results from the same mice.

In addition, the global shift was non-homogeneous, indicating that rcfMRI in mice can be useful for measuring per-voxel changes in brain metabolism. Observed local differences included a cortical-subcortical difference that was similar to what was observed in CBF in humans under dexmedetomidine,[22] and also potential greater activation of the auditory cortex in the awake state due to acoustic scanner noise.

Our results thus suggest that per-voxel mapping of calibrated fMRI is possible in the preclinical mouse model. Further study is needed to apply this preclinical imaging tool, as well as to determine translation to human subjects.

Supporting information

All relevant data are available from the authors and included in the manuscript or supplementary information. Supplementary Figures S1–S7 and supplementary Tables S1–S3 are included in the supplementary information. Correspondence and requests for materials should be addressed to gthompson@shanghaitech.edu.cn or zliang@ion.ac.cn.

Funding

The author(s) disclosed receipt of the following financial support for the research, authorship, and/or publication of this article: The authors acknowledge financial support from ShanghaiTech University, the Shanghai Municipal Government, and the National Natural Science Foundation of China Grant 81950410637 (GJT) and Grant 81771821 (ZL), Strategic Priority Research Program of the Chinese Academy of Sciences (Grant No. XDB32030100 to ZL), the Shanghai Municipal Science and Technology Major Project (Grant No. 2018SHZDZX05 to ZL) and CAS Pioneer Hundred Talents Program (to ZL). Peter Herman and Fahmeed Hyder at Yale University were supported by R01 NS-100106, R01 MH-111424, and R01 DC-014723-05S1 from NIH. The funding sources did not contribute to the writing of this manuscript.

Acknowledgments

Mengyang Xu thanks Xingyu Zhou from Vanderbilt University for his helpful disscussion for our work and Bowen Shi for transcription. Garth Thompson, Peter Herman, and Fahmeed Hyder thank Naomi Driesen from Yale University for helpful discussion of calibrated fMRI in the human brain.

Declaration of conflicting interests

The author(s) declared no potential conflicts of interest with respect to the research, authorship, and/or publication of this article.

Authors' contributions

MX and BB contributed equally. MX and GJT planned and designed the experiment. BB conducted the animal experiments. MX and BB conducted data analysis and wrote the first draft. MP and YC assisted with animal experiments. CYS assisted with experiment planning, equation development, and writing. QQ assisted with data analysis and writing. LH, JMW, ELB, ZW, and HL provided MRI sequences and helped with writing. PH and FH assisted with experiment planning, equation development, and writing. ZJL supervised MX and GJT. ZL and GJT supervised the animal experiments, data analysis, and writing.

ORCID iDs

Mengyang Xu https://orcid.org/0000-0003-1346-1191
Qikai Qin https://orcid.org/0000-0002-8826-5171
Lydiane Hirschler https://orcid.org/0000-0003-2379-0861
Jan M Warnking https://orcid.org/0000-0002-1683-5163
Hanzhang Lu https://orcid.org/0000-0003-3871-1564

Supplemental material

Supplemental material for this article is available online.

References

1. Soares JM, Magalhaes R, Moreira PS, et al. A hitchhiker's guide to functional magnetic resonance imaging. *Front Neurosci* 2016; 10: 515.
2. Thompson GJ. Neural and metabolic basis of dynamic resting state fMRI. *NeuroImage* 2018; 180: 448–462.
3. Ogawa S, Menon RS, Tank DW, et al. Functional brain mapping by blood oxygenation level-dependent contrast magnetic resonance imaging. A comparison of signal characteristics with a biophysical model. *Biophys J* 1993; 64: 803–812.
4. Hyder F, Kida I, Behar KL, et al. Quantitative functional imaging of the brain: towards mapping neuronal activity by BOLD fMRI. *NMR Biomed* 2001; 14: 413–431.
5. Mandino F, Cerri DH, Garin CM, et al. Animal functional magnetic resonance imaging: trends and path toward standardization. *Front Neuroinform* 2019; 13: 78.
6. Sanganahalli BG, Herman P, Rothman DL, et al. Metabolic demands of neural-hemodynamic associated

and disassociated areas in brain. *J Cereb Blood Flow Metab* 2016; 36: 1695–1707.
7. Herman P, Sanganahalli BG, Blumenfeld H, et al. Quantitative basis for neuroimaging of cortical laminae with calibrated functional MRI. *Proc Natl Acad Sci USA* 2013; 110: 15115–15120.
8. Maandag NJ, Coman D, Sanganahalli BG, et al. Energetics of neuronal signaling and fMRI activity. *Proc Natl Acad Sci USA* 2007; 104: 20546–20551.
9. Sanganahalli BG, Herman P, Blumenfeld H, et al. Oxidative neuroenergetics in event-related paradigms. *J Neurosci* 2009; 29: 1707–1718.
10. Davis TL, Kwong KK, Weisskoff RM, et al. Calibrated functional MRI: mapping the dynamics of oxidative metabolism. *Proc Natl Acad Sci USA* 1998; 95: 1834–1839.
11. Hoge RD, Atkinson J, Gill B, et al. Investigation of BOLD signal dependence on cerebral blood flow and oxygen consumption: the deoxyhemoglobin dilution model. *Magn Reson Med* 1999; 42: 849–863.
12. Chiarelli PA, Bulte DP, Wise R, et al. Calibration method for quantitative BOLD fMRI based on hyperoxia. *NeuroImage* 2007; 37: 808–820.
13. Hoge RD. Calibrated FMRI. *NeuroImage* 2012; 62: 930–937.
14. Kida I, Kennan RP, Rothman DL, et al. High-resolution CMR(O2) mapping in rat cortex: a multiparametric approach to calibration of BOLD image contrast at 7 tesla. *J Cereb Blood Flow Metab* 2000; 20: 847–860.
15. Shu CY, Herman P, Coman D, et al. Brain region and activity-dependent properties of M for calibrated fMRI. *NeuroImage* 2016; 125: 848–856.
16. Berman AJL, Mazerolle EL, MacDonald ME, et al. Gas-free calibrated fMRI with a correction for vessel-size sensitivity. *NeuroImage* 2018; 169: 176–188.
17. Liu EY, Guo J, Simon AB, et al. The potential for gas-free measurements of absolute oxygen metabolism during both baseline and activation states in the human brain. *NeuroImage* 2020; 207: 116342.
18. Blockley NP, Griffeth VE and Buxton RB. A general analysis of calibrated BOLD methodology for measuring CMRO2 responses: comparison of a new approach with existing methods. *NeuroImage* 2012; 60: 279–289.
19. Rodgers ZB, Detre JA and Wehrli FW. MRI-based methods for quantification of the cerebral metabolic rate of oxygen. *J Cereb Blood Flow Metab* 2016; 36: 1165–1185.
20. Slupe AM and Kirsch JR. Effects of anesthesia on cerebral blood flow, metabolism, and neuroprotection. *J Cereb Blood Flow Metab* 2018; 38: 2192–2208.
21. Drummond JC, Dao AV, Roth DM, et al. Effect of dexmedetomidine on cerebral blood flow velocity, cerebral metabolic rate, and carbon dioxide response in normal humans. *Anesthesiology* 2008; 108: 225–232.
22. Prielipp RC, Wall MH, Tobin JR, et al. Dexmedetomidine-induced sedation in volunteers decreases regional and global cerebral blood flow. *Anesth Analg* 2002; 95: 1052–1059. table of contents.
23. Grandjean J, Schroeter A, Batata I, et al. Optimization of anesthesia protocol for resting-state fMRI in mice based on differential effects of anesthetics on functional connectivity patterns. *NeuroImage* 2014; 102 Pt 2: 838–847.
24. Han Z, Chen W, Chen X, et al. Awake and behaving mouse fMRI during go/no-go task. *NeuroImage* 2019; 188: 733–742.
25. Sicard KM and Duong TQ. Effects of hypoxia, hyperoxia, and hypercapnia on baseline and stimulus-evoked BOLD, CBF, and CMRO2 in spontaneously breathing animals. *NeuroImage* 2005; 25: 850–858.
26. Shu CY, Sanganahalli BG, Coman D, et al. Quantitative beta mapping for calibrated fMRI. *NeuroImage* 2016; 126: 219–228.
27. Lu H, Xu F, Grgac K, et al. Calibration and validation of TRUST MRI for the estimation of cerebral blood oxygenation. *Magn Reson Med* 2012; 67: 42–49.
28. Wei Z, Xu J, Liu P, et al. Quantitative assessment of cerebral venous blood T2 in mouse at 11.7T: implementation, optimization, and age effect. *Magn Reson Med* 2018; 80: 521–528.
29. Shu CY, Sanganahalli BG, Coman D, et al. New horizons in neurometabolic and neurovascular coupling from calibrated fMRI. *Prog Brain Res* 2016; 225: 99–122.
30. Boxerman JL, Bandettini PA, Kwong KK, et al. The intravascular contribution to fMRI signal change: Monte Carlo modeling and diffusion-weighted studies in vivo. *Magn Reson Med* 1995; 34: 4–10.
31. Silvennoinen MJ, Clingman CS, Golay X, et al. Comparison of the dependence of blood R2 and R2* on oxygen saturation at 1.5 and 4.7 tesla. *Magn Reson Med* 2003; 49: 47–60.
32. Grubb RL, Raichle ME, Eichling JO, et al. Ter-Pogossian MM. The effects of changes in PaCO2 on cerebral blood volume, blood flow, and vascular mean transit time. *Stroke* 1974; 5: 630–639.
33. *Laboratory animal – Guideline for ethical review of animal welfare*. GB/T 35892-2018 China: National Standards of the People's Republic of China, 2018.
34. Laboratory animal – Guideline for ethical review of animal welfare, http://www.gb688.cn/bzgk/gb/newGbInfo?hcno=9BA619057D5C13103622A10FF4BA5D14. (accessed 11 November 2021).
35. Percie Du Sert N, Hurst V, Ahluwalia A, et al. The ARRIVE guidelines 2.0: updated guidelines for reporting animal research. *J Cereb Blood Flow Metab* 2020; 40: 1769–1777.
36. Chen X, Tong C, Han Z, et al. Sensory evoked fMRI paradigms in awake mice. *NeuroImage* 2020; 204: 116242.
37. Kobayashi M, Mori T, Kiyono Y, et al. Cerebral oxygen metabolism of rats using injectable (15)O-oxygen with a steady-state method. *J Cereb Blood Flow Metab* 2012; 32: 33–40.
38. Watabe T, Shimosegawa E, Watabe H, et al. Quantitative evaluation of cerebral blood flow and oxygen metabolism in normal anesthetized rats: 15O-labeled gas inhalation PET with MRI fusion. *J Nucl Med* 2013; 54: 283–290.
39. Fukuda M, Vazquez AL, Zong X, et al. Effects of the α_2-adrenergic receptor agonist dexmedetomidine on neural,

vascular and BOLD fMRI responses in the somatosensory cortex. *Eur J Neurosci* 2013; 37: 80–95.
40. Hirschler L, Munting LP, Khmelinskii A, et al. Transit time mapping in the mouse brain using time-encoded pCASL. *NMR Biomed* 2018; 31: e3855.
41. Wang Z, Aguirre GK, Rao H, et al. Empirical optimization of ASL data analysis using an ASL data processing toolbox: ASLtbx. *Magnetic Reson Imaging* 2008; 26: 261–269.
42. Hyder F, Herman P, Bailey CJ, et al. Uniform distributions of glucose oxidation and oxygen extraction in gray matter of normal human brain: no evidence of regional differences of aerobic glycolysis. *J Cereb Blood Flow Metab* 2016; 36: 903–916.
43. Carvajal-Rodriguez A and de Una-Alvarez J. Assessing significance in high-throughput experiments by sequential goodness of fit and q-value estimation. *PloS One* 2011; 6: e24700.
44. Xiong B, Li A, Lou Y, et al. Precise cerebral vascular atlas in stereotaxic coordinates of whole mouse brain. *Front Neuroanat* 2017; 11: 128.
45. Dorr A, Sled JG and Kabani N. Three-dimensional cerebral vasculature of the CBA mouse brain: a magnetic resonance imaging and micro computed tomography study. *NeuroImage* 2007; 35: 1409–1423.
46. Kida I, Rothman DL and Hyder F. Dynamics of changes in blood flow, volume, and oxygenation: implications for dynamic functional magnetic resonance imaging calibration. *J Cereb Blood Flow Metab* 2007; 27: 690–696.
47. Chen JJ and Pike GB. MRI measurement of the BOLD-specific flow-volume relationship during hypercapnia and hypocapnia in humans. *NeuroImage* 2010; 53: 383–391.
48. Lee SP, Duong TQ, Yang G, et al. Relative changes of cerebral arterial and venous blood volumes during increased cerebral blood flow: implications for BOLD fMRI. *Magn Reson Med* 2001; 45: 791–800.
49. Ciris PA, Qiu M and Constable RT. Non-invasive quantification of absolute cerebral blood volume during functional activation applicable to the whole human brain. *Magn Reson Med* 2014; 71: 580–590.
50. Alkire MT, Gruver R, Miller J, et al. Neuroimaging analysis of an anesthetic gas that blocks human emotional memory. *Proc Natl Acad Sci USA* 2008; 105: 1722–1727.
51. Alkire MT, Haier RJ, Shah NK, et al. Positron emission tomography study of regional cerebral metabolism in humans during isoflurane anesthesia. *Anesthesiology* 1997; 86: 549–557.
52. Alkire MT, Pomfrett CJ, Haier RJ, et al. Functional brain imaging during anesthesia in humans: effects of halothane on global and regional cerebral glucose metabolism. *Anesthesiology* 1999; 90: 701–709.
53. Schlunzen L, Vafaee MS, Cold GE, et al. Effects of subanaesthetic and anaesthetic doses of sevoflurane on regional cerebral blood flow in healthy volunteers. A positron emission tomographic study. *Acta Anaesthesiol Scand* 2004; 48: 1268–1276.
54. Schlunzen L, Juul N, Hansen KV, et al. Regional cerebral glucose metabolism during sevoflurane anaesthesia in healthy subjects studied with positron emission tomography. *Acta Anaesthesiol Scand* 2010; 54: 603–609.
55. Hyder F, Fulbright RK, Shulman RG, et al. Glutamatergic function in the resting awake human brain is supported by uniformly high oxidative energy. *J Cereb Blood Flow Metab* 2013; 33: 339–347.
56. Uhrig L, Ciobanu L, Djemai B, et al. Sedation agents differentially modulate cortical and subcortical blood oxygenation: evidence from ultra-high field MRI at 17.2 T. *PloS One* 2014; 9: e100323.
57. Liu X, Rabin PL, Yuan Y, et al. Effects of anesthetic and sedative agents on sympathetic nerve activity. *Heart Rhythm* 2019; 16: 1875–1882.
58. Lee C and Jones TA. Effects of ketamine compared with urethane anesthesia on vestibular sensory evoked potentials and systemic physiology in mice. *J Am Assoc Lab Anim Sci* 2018; 57: 268–277.
59. Tang CY and Ramani R. fMRI and anesthesia. *Int Anesthesiol Clin* 2016; 54: 129–142.
60. Mortensen KN, Gjedde A, Thompson GJ, et al. Impact of global mean normalization on regional glucose metabolism in the human brain. *Neural Plast* 2018; 2018: 6120925.
61. Dienel GA. Brain glucose metabolism: integration of energetics with function. *Physiol Rev* 2019; 99: 949–1045.
62. Qiu G, Wu Y, Yang Z, et al. Dexmedetomidine activation of dopamine neurons in the ventral tegmental area attenuates the depth of sedation in mice. *Anesthesiology* 2020; 133: 377–392.
63. Kim WH, Cho D, Lee B, et al. Changes in brain activation during sedation induced by dexmedetomidine. *J Int Med Res* 2017; 45: 1158–1167.
64. Ganjoo P, Farber NE, Hudetz A, et al. In vivo effects of dexmedetomidine on laser-Doppler flow and pial arteriolar diameter. *Anesthesiology* 1998; 88: 429–439.
65. Pan WJ, Billings JC, Grooms JK, et al. Considerations for resting state functional MRI and functional connectivity studies in rodents. *Front Neurosci* 2015; 9: 269.
66. Sinclair MD. A review of the physiological effects of alpha2-agonists related to the clinical use of medetomidine in small animal practice. *Can Vet J* 2003; 44: 885–897.
67. Reiz S, Bålfors E, Sørensen MB, et al. Isoflurane–a powerful coronary vasodilator in patients with coronary artery disease. *Anesthesiology* 1983; 59: 91–97.
68. Warkander DE, Shykoff BE. Combinations of Breathing Resistance and Inspired CO_2: Effects on Exercise Endurance. *Navy Experimental Diving Unit, Panama City*, FL, 2015; NEDU TR 14–14.
69. Xu F, Uh J, Brier MR, et al. The influence of carbon dioxide on brain activity and metabolism in conscious humans. *J Cereb Blood Flow Metab* 2011; 31: 58–67.
70. Otis AB and Rahn H. Performance as related to composition of alveolar air. *Am J Physiol* 1946; 146: 207–221.
71. Dulla CG, Dobelis P, Pearson T, et al. Adenosine and ATP link PCO2 to cortical excitability via pH. *Neuron* 2005; 48: 1011–1023.

72. Zappe AC, Uludag K, Oeltermann A, et al. The influence of moderate hypercapnia on neural activity in the anesthetized nonhuman primate. *Cerebral Cortex (New York, N.Y.: 1991)* 2008; 18: 2666–2673.
73. Göttler J, Kaczmarz S, Kallmayer M, et al. Flow-metabolism uncoupling in patients with asymptomatic unilateral carotid artery stenosis assessed by multi-modal magnetic resonance imaging. *J Cereb Blood Flow Metab* 2019; 39: 2132–2143.
74. Janke AL, Ullmann JFP. Robust methods to create ex vivo minimum deformation atlases for brain mapping. *Methods* 2015; 73: 18–26.